Demonstration of Emittance Compensation through the Measurement of the Slice Emittance of a 10-ps Electron Bunch

X. Qiu, K. Batchelor, I. Ben-Zvi, and X-J. Wang

National Synchrotron Light Source Department, Brookhaven National Laboratory, Upton, New York 11973

(Received 23 October 1995)

The beam matrix of a picosecond long slice of an electron bunch was measured. A short slice is selected out of an energy chirped beam by a slit in a dispersive region. The emittance is measured using the quadrupole scan technique. We observe the process of emittance compensation of the beam by repeating the measurement for various values of the compensating solenoid and for several slices. [S0031-9007(96)00194-9]

PACS numbers: 29.27.Fh, 41.85.Si

Less than a decade ago, Carlsten [1] proposed that the observed emittance growth due to linear components of space charge forces in a photocathode RF electron gun can be compensated. This emittance growth is due to a misalignment of the phase space ellipses of short longitudinal sections of the electron beam bunch (slices). His compensation technique uses a solenoid lens to produce a laminar-flow beam-waist downstream of the gun. The space-charge interaction in the beam waist rotates the slice ellipses differentially to counter the original rotation and to produce alignment downstream of the waist. As shown since in numerous experiments [2–4], this technique resulted in a large improvement in the brightness of electron beams so significant for e^+e^- linear colliders and short wavelength free-electron lasers.

In the past, emittance compensation has been observed by measuring the reduction of this total projected emittance. We present here the first measurement of the relative rotation of the slice ellipses leading to emittance compensation. We do this by dissecting the electron bunch longitudinally into slices on a picosecond time scale. The emittance and orientation of the phase space ellipse are measured for each individual slice by the quadrupole magnet scan technique. We repeat this measurement for a number of field settings of the solenoid, and show that the phase space ellipse of the slices indeed rotate relative to each other as the solenoid field is changed, and go through near alignment at a particular solenoid field.

The measurement was done with the one-and-half cell *S*-band laser-photocathode RF gun of the BNL Accelerator Test Facility. Figure 1 is a schematic of the experiment. The beam is generated at the photocathode by a 10-ps (FWHM) long UV laser pulse. The electron bunch, with a charge of 0.4 nC, is rapidly accelerated in the twin cells of the gun's RF cavity by a 89 MV/m peak electrical field to an energy of 4 MeV. The beam emerging from the gun is focused by a solenoid magnet and injected into a 2856 MHz linear accelerator (linac). A laminar-flow beam waist is formed in the linac, during acceleration. The acceleration continues until the space-charge forces become negligibly small, freezing the resultant phase space distribution. The linac consists of two sections. The phase of the second section is controlled independently by a motor controlled phase shifter. The high energy beam is bent horizontally by a 20° dipole magnet and a small slice in energy is selected by a slit. A quadrupole magnet following the slit is scanned in current and the vertical beam size is measured on a beam profile monitor (BPM). The BPM comprises a phosphorous screen to form a luminous image of the beam intensity profile and a charge coupled device (CCD) camera to record it. The distance from the quadrupole to the BPM is 8.96 m. For clarity we omit from the figure various beam transport quadrupole lenses in the high energy beam line.

The second linac section, dipole, and slit form a filter that passes only a short slice of the beam pulse downstream of the slit. The quadrupole lenses and beam profile monitor downstream of the filter form a analyzer to measure the beam matrix of the slice. The filter is tuned to a given slice by changing the phase of the second linac

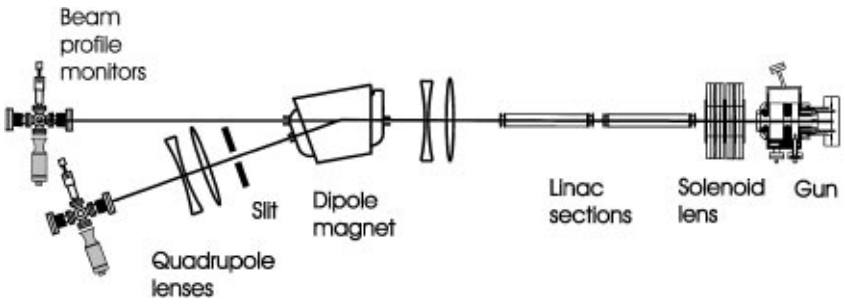

FIG. 1. Schematic diagram of the experimental setup (not to scale).

section. Since the dipole current is constant, the energy of a selected slice is constant regardless of its position along the bunch, and the optics of the selected slices in the filter (and before it) are identical. However, under regular operation of the machine the slices enter the second linac section at slightly different phases around the crest of the accelerating wave form. Thus they will experience a slightly different focusing. The maximum relative defocusing kick along a 10-ps long bunch positioned at the crest is of the order of half a microradian. This is 2 orders of magnitude smaller than the angular spread in the approximately 1 mm diameter beam as it enters the second linac section and thus negligible.

The experimental data were obtained by the BPM. The image of the beam is captured by a CCD camera (Pulnix model 745E) with a frame grabber (Spiricon model LBA-100A). The CCD camera has pixel size of 11 by 13 μm and the number of pixels is 512 by 480. A remotely controlled iris is used to avoid saturation in the 8 bit dynamic range of the frame grabber. The Gd_2O_2S:Tb phosphor is linear in light per charge output under our beam energy and charge conditions. The spatial resolution of the light emanating from the phosphor is better than 100 μm; thus our resolution is determined by a combination of the pixel size and the phosphor resolution. This resolution is the basis for the error estimate in the emittance measurements. The digitized image from the frame grabber was written onto a diskette to be analyzed off-line. The analysis consists of integrating over the horizontal direction and obtaining the rms beam size for the vertical direction. Each vertical rms size corresponds to one point in a quadrupole scan.

At the beginning of the measurement the electron bunch was positioned at the crest of the RF wave form in both linac sections. The beam energy was then 52 MeV. The energy spread was estimated by measuring the size of the beam on the phosphor coated slit (using a CCD camera) and applying the 5.3 mm/% dispersion at the slit. The horizontal spot size on the slit is determined by the beta function at that point and by the energy spread. The latter is a combination of the curvature of the accelerating field over the bunch length and the local (per slice) energy spread. The measured horizontal spot size was equivalent to an energy spread of 0.5%. The slit opening was adjusted to an opening of 2.6 mm equivalent to an energy bite of about 0.5%. Next, the second linac section was dephased by 29.8 deg to produce a nearly linear energy chirp of 0.439% per picosecond. The total energy was reduced from 52 to 48.8 MeV. Because of this chirp, the slit opening corresponded to 1.1 ps. The beam passed by the slit averaged a slightly larger time slice due to the small horizontal betatron size at the slit. The phase offset (at a constant dipole current) filters a given beam slice to the analyzer.

The longitudinal charge distribution of the electron beam bunch is shown in Fig. 2, with arrows indicating

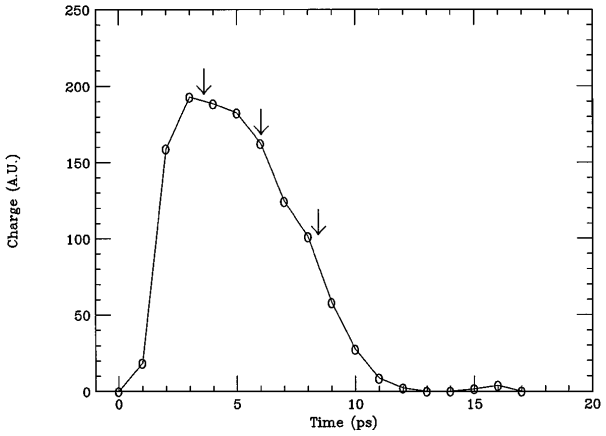

FIG. 2. The longitudinal charge distribution of the electron beam bunch.

the position of the three slices used in our measurement. The slice phase space evolution depends on its current and its position in the bunch, but we have avoided the steep leading edge of the bunch because of the sensitivity to timing jitter at the point. For each solenoid field setting, the vertical beam size was measured as the function of the scanning quadrupole magnet current. Each plot in Fig. 3 represents one field setting of the solenoid. The discrete data points are marked and best fit curves to the data of each slice are plotted. The curves represent the calculated beam size at the BPM using the calibrated quadrupole strength as a function of current and the known drift length from the quadrupole to the BPM. The beam matrix at the entrance of the quadrupole represents three parameters that are the variables in a best fit procedure.

If the coupling among different dimensions is negligible, the particle distribution in the vertical plane (specifying the emittance, ellipse aspect ratio, and orientation) is represented by a symmetric beam matrix

$$\sigma = \begin{pmatrix} \sigma_{11} & \sigma_{12} \\ \sigma_{21} & \sigma_{22} \end{pmatrix},$$

where $\sigma_{12} = \sigma_{21}$ is the correlation, $\sqrt{\sigma_{11}}$ is the beam size, and $\sqrt{\sigma_{22}}$ is the beam divergence. For the emittance measurement using the quadrupole magnet scan technique, the measured beam size σ_{11}^m at the beam profile monitor is connected to the beam matrix at the entrance of the varying quadrupole magnet by

$$\sigma_{11}^m = R_{11}^2\sigma_{11} + 2R_{11}R_{12}\sigma_{12} + R_{12}^2\sigma_{22},$$

where R is the beam transfer matrix from the quadrupole magnet entrance to the beam profile monitor. The beam matrix at the entrance of the quadrupole represents three parameters that are the variables in a best fit procedure.

The raw quadrupole scan data are shown in Fig. 3. Clearly the various beam slices can be made more similar by adjusting the solenoid field (current). Figure 3(a) is at a solenoid current of 102 A. This is a less than optimal solenoid current. Figure 3(b) at 106 A is closer

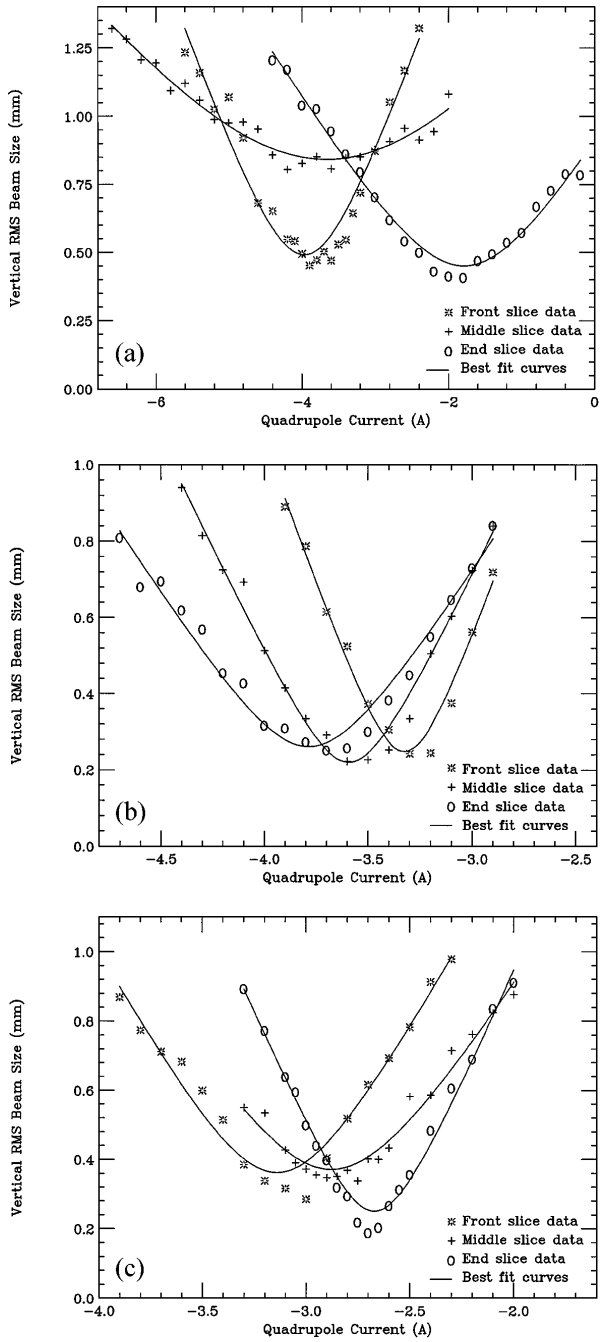

FIG. 3. Slice rms beam size as a function of the quadrupole current for the front, middle, and end slices at various solenoid currents: (a) 102 A, (b) 106 A, and (c) 110 A. The curves represent the best fit to the data points.

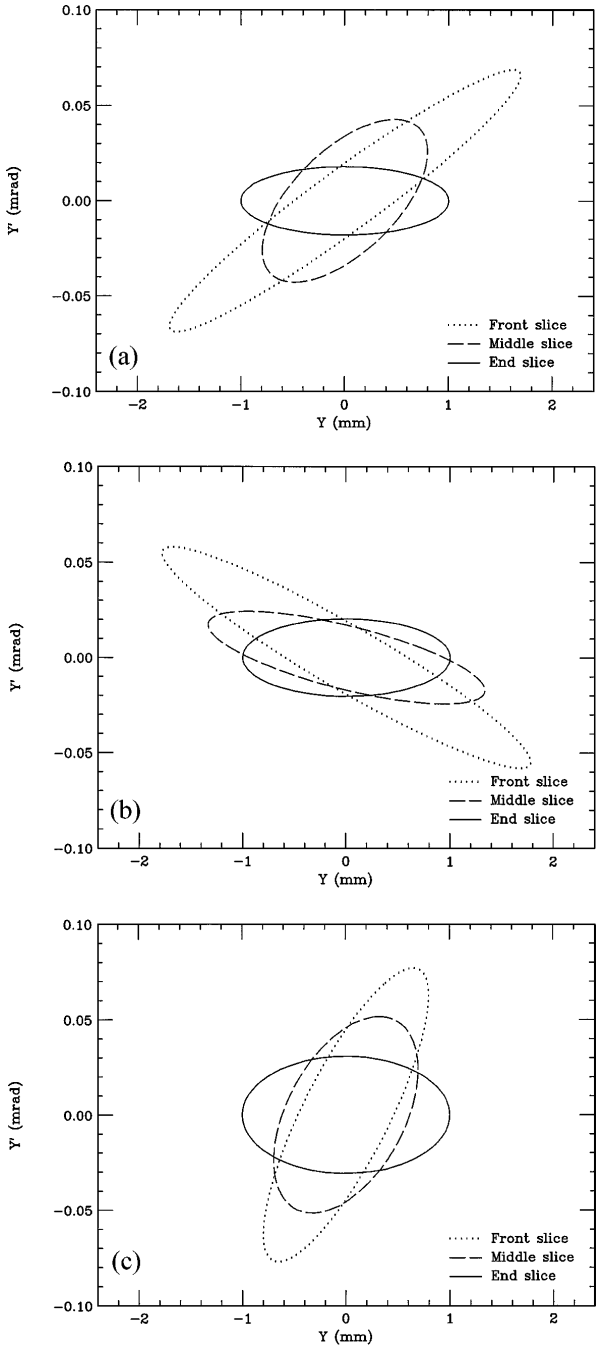

FIG. 4. Plots of the transverse phase space ellipses for each slice. The solenoid currents are (a) 102 A, (b) 106 A, and (c) 110 A.

to optimum. Figure 3(c) at 110 A is again further from optimal solenoid field.

To interpret the data better, we make the usual approximation that the beam is represented in transverse phase space by an ellipse with a given area, inclination angle, and eccentricity. These parameters (or the corresponding beam matrix) can be calculated from the best fit curve of the quadrupole scan data. The area of the ellipse is the emittance. The measured normalized rms emittances of the three slices are 3.5 ± 1.1, 2.8 ± 1.1, and 2.3 ± 1.1 for the front, center, and end slices, respectively. Within the experimental error the slice emittance does not change with the solenoid field, as expected. The variation in the overall emittance results only from the alignment of the ellipses. The measured values are rms emittances which are larger than what one would get by making the more

common full width at half maximum measurements [5] by a factor of 2 to 4. Furthermore, the emittance is larger than optimum since the laser beam spot on the cathode was smaller than optimum for the extracted charge.

In Fig. 4 we show the beam ellipses of the slices. To illustrate the relative orientation between the slice ellipses, they were rotated with a known transfer matrix so that the phase space ellipse of the end slice is an erect ellipse and has a fixed beam size in each of the plots. Figure 4 shows only the relative rotation of the slice ellipses and a reversal in this differential rotation at some solenoid field does not imply an absolute reversal. The best emittance compensation is achieved when all the slice ellipses line up. This will reduce the emittance of the whole electron bunch by producing the smallest projected area, with summation weighted by the charge in each slice.

As the beam passes through the waist created by the solenoid, the ellipses of the slices rotate relative to each other since the space-charge force is not uniform along the bunch. According to Carlsten's theory, the angle of rotation is a function of the solenoid field and the charge distribution. We name the slices after their relative position in the electron bunch: front, middle, and end. As seen from Fig. 2, the front slice has the largest charge, the middle the second largest, and the end the smallest relative charge. Comparing Figs. 4(a) and 4(b) we notice that the larger charge slices rotate through the larger angle, as expected. While Fig. 4(a) (at 102 A) represents an under-rotation, Fig. 4(b) (at 106 A) represents an over-rotation (a point of near alignment was passed). As we continue to increase the solenoid current to 110 A, seen in Fig. 4(c), the relative rotation reverses itself, passing through near alignment once again. We expect that the closest alignment of the slice ellipses is attained at two solenoid currents, one between 102 and 106 A, the other between 106 and 110 A.

The relative rotation of the ellipses as a function of the solenoid field is a balance of two effects. The space-charge force (other than at a laminar-flow beam waist) defocuses the beam, resulting in a counterclockwise rotation of the higher current slices relative to the low current reference slice. Passage through the beam waist causes a clockwise rotation, in accord with Carlsten's theory. The solenoid field determines the size and location of the waist: A stronger field makes the waist smaller and moves it closer to the gun. What we observe in the analyzer is the degree of rotation that takes place before the acceleration "freezes" the phase space distribution by diminishing the space-charge force. By freezing the space-charge interaction before the waist (low solenoid field) we observe the beam in what may be called early stage. As we increase the solenoid field, we observe later stages of its evolution.

At a low solenoid field we observe a relatively large counterclockwise rotation due to the space-charge interaction in the early stage. The waist is at a high energy region of the linac and thus ineffective As the field is increased, the beam waist moves upstream and we observe first a relative clockwise rotation of the higher current slices as the Carlsten correction takes place, then again the normal counterclockwise relative rotation.

In summary, we have measured for the first time the beam matrices of a sequence of longitudinal slices of 10-ps long electron bunch. A beam filter analyzer provided the longitudinal distribution of charge with picosecond resolution and the measurement of the beam matrices of short beam slices. This measurement can be used under conditions in which the linear compensation technique of Carlsten is not adequate, expected to occur with higher beam charge. It has been suggested [6] that nonlinear emittance compensation techniques can be applied in such cases to produce higher electron beam brightness. The slice emittance measurement provides the diagnostic tool to observe and control a nonlinear emittance correction scheme.

This work was supported by Department of Energy Contract No. DE-AC02-76CH00016.

[1] B. E. Carlsten, Nucl. Instrum. Methods Phys. Res., Sect. A **285**, 313–319 (1989).

[2] D. W. Feldman *et al.,* Nucl. Instrum. Methods Phys. Res., Sect. A **304**, 224–227 (1991).

[3] D. Dowell *et al.,* in *Proceedings of the 1993 Particle Accelerator Conference* (IEEE, New York, 1993), pp. 2967–2969.

[4] X. J. Wang *et al.,* in Proceedings of the 1995 Particle Accelerator Conference, Dallas, Texas, 1995 (IEEE, New York, to be published).

[5] B. E. Carlsten, J. C. Goldstein, P. G. O'Shea, and E. J. Pitcher, Nucl. Instrum. Methods Phys. Res., Sect. A **331**, 791–796 (1993).

[6] J. C. Gallardo and R. B. Palmer, IEEE J. Quantum Electron. **26**, 1328–1331 (1990).